Available online at www.sciencedirect.com
ScienceDirect
C. R. Physique 8 (2007) 1205–1212
COMPTES RENDUS PHYSIQUE
http://france.elsevier.com/direct/COMREN/

Optical parametric sources for the infrared/Sources optiques paramétriques pour l'infrarouge

Fresnel phase matching: a universal phase matching scheme

Myriam Raybaut [a,*], Antoine Godard [a], Clement Lubin [a], Riad Haidar [a], Emmanuel Rosencher [a,b]

[a] *Office national d'études et de recherches aérospatiales (ONERA), Chemin de la Hunière, 91761 Palaiseau cedex, France*
[b] *Département de physique, École polytechnique, 91128 Palaiseau cedex, France*

Available online 29 October 2007

Abstract

We present new theoretical concepts for Fresnel phase matching. A guided wave approach is described, which allows us to intrinsically take into account all the physical processes involved. ***To cite this article: M. Raybaut et al., C. R. Physique 8 (2007).***

Résumé

Quasi-accord de phase par biréfringence de Fresnel : une technique d'accord de phase universelle. Nous présentons de nouveaux concepts théoriques pour l'accord de phase par biréfringence de Fresnel. Ces nouveaux modèles sont basés sur une approche modale, nous permettant de prendre en compte de manière intrinsèque tous les processus physiques intervenant lors de cette interaction paramétrique. ***Pour citer cet article : M. Raybaut et al., C. R. Physique 8 (2007).***

Keywords: Frequency conversion; Phase matching; Semiconductor nonlinear optics

Mots-clés : Conversion de fréquence ; Accord de phase ; Optique non linéaire dans les semiconducteurs

1. Introduction

Three waves mixing in a nonlinear optical material provide a convenient way to generate largely tunable coherent radiations, particularly in the mid-infrared regime where such sources are scarce. Three waves of complex amplitudes $\vec{E}_i(\vec{r},t) = \vec{E}_i(\vec{r})\mathrm{e}^{\mathrm{i}(\omega_i t - \vec{k}_i\vec{r})}$ exchange energy via the nonlinear susceptibility tensor $\overline{\overline{\chi}}^{(2)}$. In this latter expression, ω_i are the optical pulsations, $\vec{k}_i$ the wavevectors, $\vec{E}_i(\vec{r})$ the slowly varying envelope functions, $i = 1, 2, 3$. The energy transfer will be efficient if two conditions are met: energy and photon momentum conservation, i.e.:

$$\begin{aligned} &\omega_3 = \omega_1 + \omega_2 \\ &\Delta\vec{k} = \vec{k}_3 - \vec{k}_1 - \vec{k}_2 = 0 \end{aligned} \tag{1}$$

* Corresponding author.
E-mail address: myriam.raybaut@onera.fr (M. Raybaut).

1631-0705/$ – see front matter
doi:10.1016/j.crhy.2007.09.008

Because of optical dispersion, these two conditions cannot be naturally fulfilled. In that case, there is a growing phase lag $e^{i\Delta\vec{k}\vec{r}}$ between the three waves as they propagate and interact in the nonlinear materials. Consequently, energy will flow back and forth between the waves with a spatial periodicity given by the coherence length $\Lambda_c = \pi/\Delta k$.

Many schemes have been proposed in order to alleviate this problem [1–3]. One of the most popular one is the quasi-phase matching scheme: Every coherence length, the sign of the effective nonlinearity in the beam direction is reversed, adding a π phase to the relative phase $\Delta k \Lambda_c$ and preventing destructive interaction from taking place.

Typical coherence lengths range from few microns to few tens of microns, depending on the interacting wavelengths. The sign reversal of the materials nonlinearity thus calls for complex metallurgical processes, such as molecular bonding, patterned growth or ferroelectric poling.

In their pioneering work, Armstrong et al. proposed to use total internal reflection to provide this sign reversal of the effective nonlinearity [4]. The advantage of this technique is that it does not require complex technological processes and can be considered as universal. It is particularly useful in optically isotropic materials where birefringence phase matching is not feasible. Though attractive, this proposal has been given very little attention and stayed largely unexplored, both experimentally and theoretically [5,6]. The purpose of this article is to describe the recent developments of this technique.

2. Fresnel phase matching: a plane wave approach

In the Fresnel phase matching scenario, the interacting waves are trapped by total internal reflection in a nonlinear material, such as a cubic semiconductor (GaAs, GaP, ZnSe, ...). The fundamental waves are launched in the wafer through a bevelled facet (see Fig. 1). At total internal reflection at the air-material interface, each wave i experiences a phase change ϕ_F^i (Fresnel phase shift) which depends on their different polarisation and wavelength. Using *a simple ray description* and assuming that the *waves are collinear*, it is straightforward to demonstrate that the amount of power I_1 generated by, e.g., difference frequency between two waves of power I_3 and I_2 is given by:

$$I_1 = \frac{Z_0}{2c^2}\frac{(\omega_1 d_{\text{eff}} L N)^2}{n_1 n_2 n_3}\left(\sin c\frac{\Delta k L}{2}\right)^2 \frac{(\sin\frac{N\Delta\Phi}{2})}{(N\sin\frac{\Delta\Phi}{2})^2}^2 I_3 I_2 \tag{2}$$

In the above expression, Z_0 is the vacuum impedance (377 Ω), c is the velocity of light, N is the number of bounces in the wafer, L is the distance travelled by the beams between two bounces ($L = t/\cos\theta$ where t is the wafer thickness and θ is the propagation angle), sinc is the cardinal function ($\operatorname{sinc} x = \sin x/x$) and d_{eff} is the effective nonlinear coefficient in the direction of propagation. For instance, for the geometrical case described in Fig. 1, for different states of polarization of the waves 3, 2, 1 (s = perpendicular, p = parallel), d_{eff} can be given by:

$$\begin{aligned} d_{\text{eff spp}} &= d.\left(\frac{1}{2}\cos^2\theta.[1+3\cos 2\varphi] + \sin^2\theta\right).\sin\varphi \\ d_{\text{eff pss}} &= \frac{1}{4}d.(\cos\varphi + 3\cos 3\varphi).\cos\theta \end{aligned} \tag{3}$$

which shows that, indeed, the behaviour of d_{eff} at reflection can be rather complicated.

More importantly, $\Delta\Phi$ is the total phase shift between the interacting waves due to the contribution of: (i) the phase mismatch (ΔkL); (ii) the relative Fresnel phase shift at total internal reflection ($\Delta\phi_F = \phi_F^3 - \phi_F^1 - \phi_F^2$); and (iii) the change in the value of the effective susceptibility d_{eff} at reflection:

$$\Delta\Phi = \Delta kL + \Delta\phi_F + \varepsilon\pi \tag{4}$$

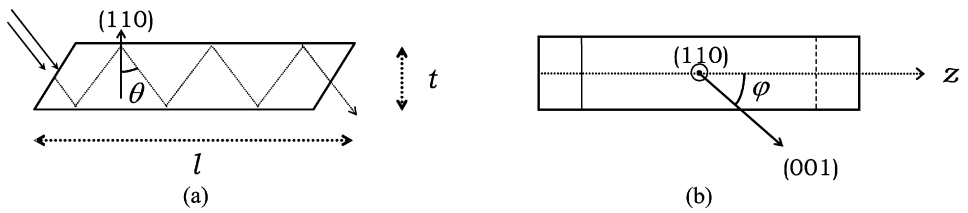

Fig. 1. Geometry of the Fresnel phase-matched plate: (a) side view for geometrical description; and (b) view from above for angle definition.

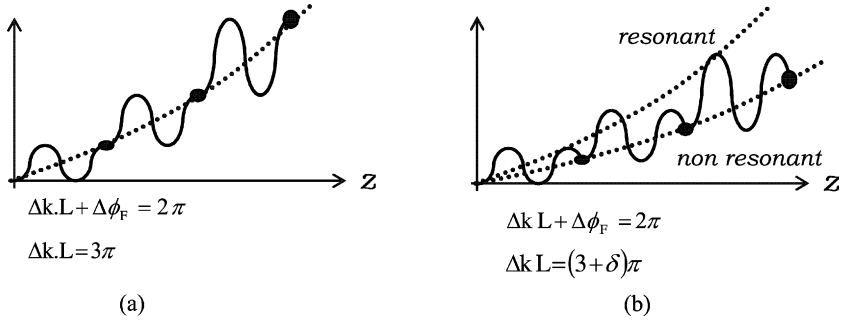

Fig. 2. Resonant (a) and nonresonant (b) Fresnel phase matching.

For instance, $\varepsilon = 0$ ($\varepsilon = 1$ respectively) if the value of d_{eff} is unchanged (reversed respectively) at reflection. Finally, the value of Fresnel phase shift ϕ_F is given by [7]:

$$\Delta\phi_F^i = -2\arctan\left(\frac{((1-q)+qn_i^2)\sqrt{n_i^2\sin^2\theta - 1}}{n_i\cos\theta}\right) \tag{5}$$

This latter expression shows that the value of the Fresnel phase shift can be fairly large (from 0 to π, particularly near the critical angle $\theta_c^i = \text{Arcsin}\frac{1}{n_i}$) so that *any phase mismatch can be compensated by a slight change in the propagation angle* θ: this is the basic idea of Fresnel phase matching.

One can notice that the phase matching conditions in expression (2) are composed of two terms: the first one describes the phase mismatch between two bounces, the second one describes the coherent summation of the parametric interaction while the waves bounce back and forth between the wafer surface. Clearly, two different kinds of phase matching occur, depending whether the two terms are resonant or not (see Fig. 2).

2.1. Resonant Fresnel phase matching (FPM)

In order to maximize both of the terms in (2), two conditions must be met:

$$\begin{aligned}&\Delta k(\omega_{1,2,3}).L(t,\theta) = m\pi\\ &\Delta\phi_F(\theta, P_{1,2,3}) + \varepsilon(\theta, P_{1,2,3})\pi = \pi\end{aligned} \tag{6}$$

where $P_{1,2,3}$ symbolizes the different polarization of the waves, and m is an odd number. In these latter equations, the influence of the optical dispersion on the Fresnel phase shift (i.e. influence of ω_i) is neglected since it is shown that they play a secondary role [6]. Fig. 3 shows a graphical solution of Eq. (6) for a given set of fundamental waves ((1.9 μm, 2.3 μm) $\underset{\text{DFG}}{\longrightarrow}$ 11 μm) in GaAs.

There are pros and cons for resonant FPM. On the one hand, this configuration yields the maximum conversion efficiency, with an amount of converted light given by:

$$I_1^{\text{out}} = \frac{2Z_0}{\pi^2c^2}\frac{(\omega_1.d_{\text{eff}})^2}{n_1n_2n_3}\Lambda_C^2N^2I_3^{\text{in}}I_2^{\text{in}} \tag{7}$$

where Λ_c is the coherence length of the parametric process and N is the number of bounces. On the other hand, for a given polarization combination and a given plate thickness t, these two conditions impose a relation between the pump, waves $\omega_{2,3}$ and the angle θ which restricts the tunability of the system [6].

2.2. Nonresonant Fresnel phase matching

In this case, a single condition must be met:

$$\Delta k(\omega_{2,3})L(\theta,t) + \Delta\phi_F(\theta, P_{1,2,3}) + \varepsilon(\theta, P_{1,2,3})\pi = \pi \tag{8}$$

Now, on the one hand, the conversion efficiency is not optimum between two bounces but the parametric conversion is still constructive while the beams bounce back and forth in the plate. On the other hand, the phase matching

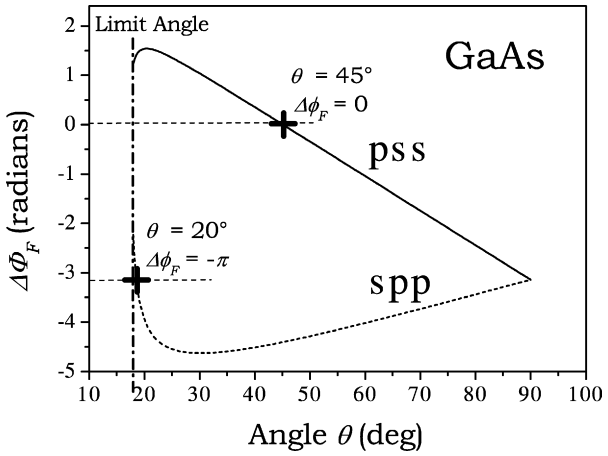

Fig. 3. Fresnel phase shift $\Delta\phi_F$ computed for various polarization configurations in GaAs plates for a (1.9 μm, 2.3 μm) $\xrightarrow[\text{DFG}]{}$ 11 μm process.

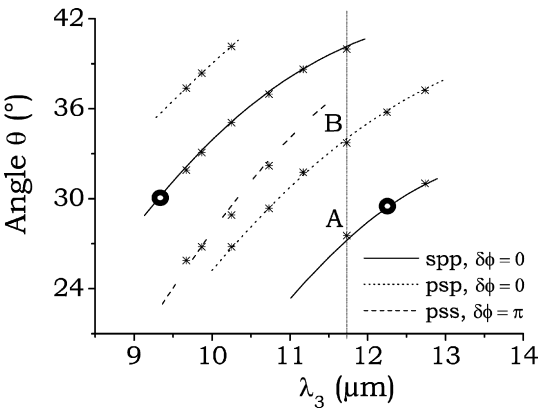

Fig. 4. A single GaAs plate is enough to cover the whole 9–13 μm spectral range. The only resonant cases are highlighted (circular points), in order to demonstrate that the hyperwide tunability is obtained thanks to the nonresonant technique.

conditions are now dramatically alleviated so that the tunability of the FPM becomes very large. Moreover, new crystallographic orientations can be phase matched in the nonresonant configuration, which can benefit from a higher effective nonlinearity d_{eff}.

Fig. 4 shows some experimental results [6]. The ω_3 and ω_2 waves are generated by a type I optical parametric oscillation in a Nd-YAG pumped $LiNbO_3$ crystal. The fine tuning is obtained by rotation of the $LiNbO_3$ crystal, whereas the linewidth narrowing (2 cm^{-1}) is achieved by a Littrow grating inside the oscillating cavity. The waves are then sent inside a GaAs semiconductor plate and generate, by difference frequency mixing, a third wave at ω_1. By tuning the values of the circular frequencies ω_1 and ω_2 inside the oscillating cavity, and rotating the GaAs plate to the adequate Fresnel phase-matching angle, nonresonant FPM allows to continuously tune the ω_3 signal from 7 to 13 μm. The different polarization configurations are indicated in the inset (s = perpendicular, p = parallel). As shown in this figure, only two sets of values would have been obtained in the resonant FPM scheme, thus highlighting the great interest in the nonresonant configuration. Fresnel phase matching has been implemented in GaAs, GaP, ZnSe [6] without any problem, showing the universal character of this phase matching scheme.

2.3. Fresnel phase matching—basic limitations

Fig. 5 shows the experimental and theoretical FPM conversion efficiency as a function of the GaAs plate length. Clearly, the efficiency does not grow quadratically with the sample length, as expected from Eq. (7) and even exhibits a maximum. In fact, three different effects are mainly involved in this phenomenon:

(i) Goos–Hänchen shifts [8]: at total internal reflection, the waves penetrate in the forbidden region (evanescent wave in the air) and emerge back in the plate at a different place (see Fig. 6(a)). The shift is a function of the wavelength and the polarization so that the three waves walk off gradually as they propagate in the plate (Fig. 6(b)).

(ii) Nonlinear reflection [9]: because of the conservation of the k vector parallel to the surface, the nonlinear waves generated at the interfaces are reflected at a different angle than the fundamental ones. For instance for second harmonic generation, assuming plane waves, the nonlinear law of reflection reads:

$$n_\omega \sin\theta_\omega = n_{2\omega} \sin\theta_{2\omega} \tag{9}$$

with obvious notations, so that there is a noncollinear angle $\delta\theta$ between the beams given by:

$$\delta\theta \approx -\frac{\delta n}{n} \operatorname{tg} \theta_\omega \tag{10}$$

This noncollinear angle is typically in the few degrees, leading also to a walk-off between the waves (see Fig. 7).

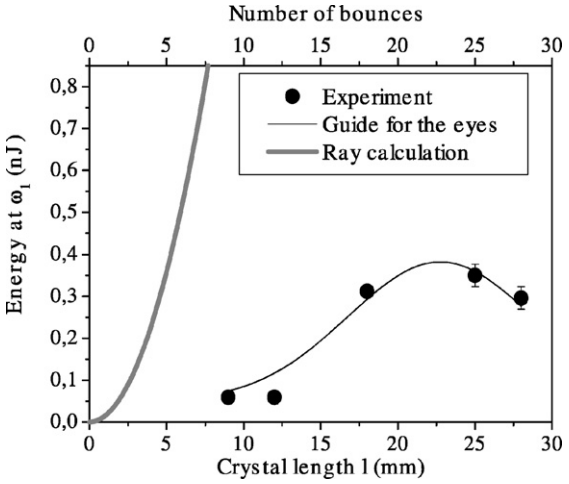

Fig. 5. Evolution of the amount of DFG power extracted from a GaAs plate as a function of the plate length for a (1.9 μm, 2.3 μm) $\underset{\text{DFG}}{\longrightarrow}$ 11 μm process: comparison between the experimental points and the plane wave theory.

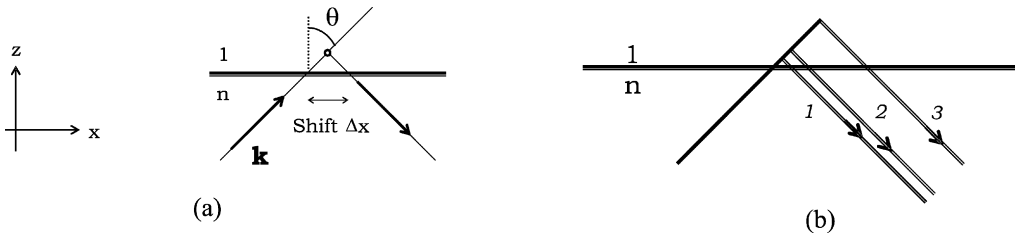

Fig. 6. (a) The Goos–Hanchen effect and (b) Effect of the Goos–Hänchen shift on the three interacting waves ('walk-off' effect).

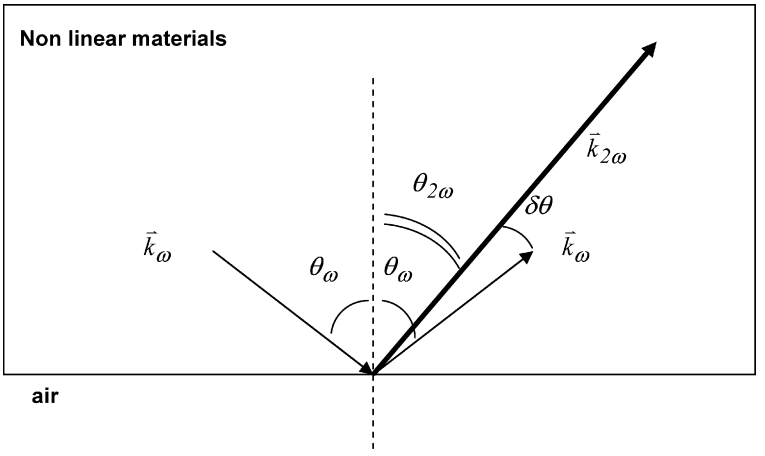

Fig. 7. Nonlinear total internal reflection.

(iii) Finally, diffraction is important and also contributes to the loss of collinearity between the waves.

All these effects are extremely difficult to take into account in the plane wave approach, but are naturally described in a guided wave approach.

3. Fresnel phase matching: a guided wave approach

It might seem ironic to call for a guided wave approach since the plate thickness is so large compared to the interacting beam wavelengths. Indeed, the plates are typically few 100 s of micron thick for 1 μm optical beam wavelength, so that hundreds of modes are envisaged. However, a straightforward calculation shows that, for Gaussian beams, only 5 to 10 modes are actually excited in the plate so that the guided wave calculation for the three waves mixing is feasible on a desktop computer. Moreover, once again, this is the only approach which can take into account such effects as Goos–Hanchen shifts, nonlinear reflection and diffraction *in a build-in way*. We illustrate the formalism in a $\mathrm{TE}_\omega \to \mathrm{TE}_{2\omega}$ second harmonic generation (SHG) situation.

The pump and SHG electric field distributions functions are respectively given by:

$$\vec{E}_y^{\omega}(x,z,t) = \sum_l A_{l,y}^{\omega}(z) E_{l,y}^{\omega}(x) \mathrm{e}^{\mathrm{i}(\omega t - \beta_l^{\omega} z)} \vec{e}_y + cc \tag{11}$$

and

$$\vec{E}_y^{2\omega}(x,z,t) = \sum_m A_{m,y}^{2\omega}(z) E_{m,y}^{2\omega}(x) \mathrm{e}^{\mathrm{i}(2\omega t - \beta_m^{2\omega} z)} \vec{e}_y + cc \tag{12}$$

In these expressions, $E_{l,y}^{\omega}(x)$ are the lth single mode TE wave functions, solutions of the linear Maxwell equations [10]. For instance, the propagation constant β_l^{ω} is solution of the implicit equation:

$$\tan\left(\alpha_l^{\omega_t}\right) = 2\frac{\kappa_l^{\omega}\alpha_l^{\omega}}{(\alpha_l^{\omega})^2 - (\kappa_l^{\omega})^2} \tag{13}$$

where $\alpha_l^{\omega} = \sqrt{(n_\omega k_\omega)^2 - \beta_l^{\omega^2}}$ and $\kappa_l^{\omega} = \sqrt{\beta_l^{\omega^2} - k_\omega^2}$ are the transverse and the evanescence wavenumber respectively. In a ray tracing interpretation, it corresponds to a zigzag angle θ_l^{ω} (with the same geometry as Fig. 8(a)) given by: $\sin\theta_l^{\omega} = \frac{\beta_l^{\omega}}{n_\omega k_\omega}$. The $A_l^{\omega}(z)$ are the slowly varying amplitudes of the fundamental modes. Their value at $z = 0$ is obtained by the projection of the input Gaussian field on the waveguide modes.

In the undepleted pump approximation ($A_l^{\omega}(z) \approx A_l^{\omega}(0) = A_l^{\omega}$), the mode coupling equation which describes the energy transfer between the fundamental and the harmonic wave is easily derived [11]:

$$A_{m,x}^{2\omega}(z) = -\frac{\omega\varepsilon_0}{p_0}\chi_{yyy}^{(2)} \sum_{l'}\sum_{l} S_{l,l',m}\left(A_{l,y}^{\omega}A_{l',y}^{\omega}\right) L\left(\frac{\mathrm{e}^{\mathrm{i}\delta\beta_{l,l',m}L} - 1}{\delta\beta_{l,l',m}L}\right) \tag{14}$$

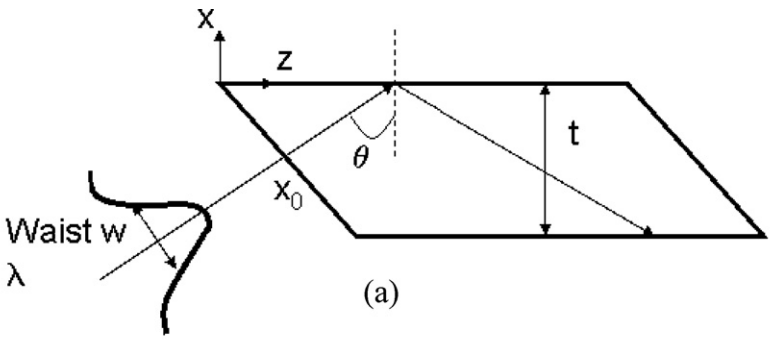

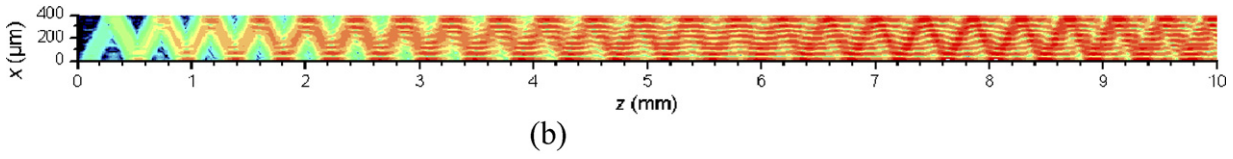

Fig. 8. (a) Geometry of the GaAs plate as a highly multimode planar waveguide, (b) Evolution of the amount of SHG (8 μm) $\underset{\text{SHG}}{\longrightarrow}$ 4 μm power as a function of distance in a GaAs plate (log scale). One clearly sees that the SGH gradually fills the plate while Goos–Hänchen shift and nonlinear reflection walk off the beams.

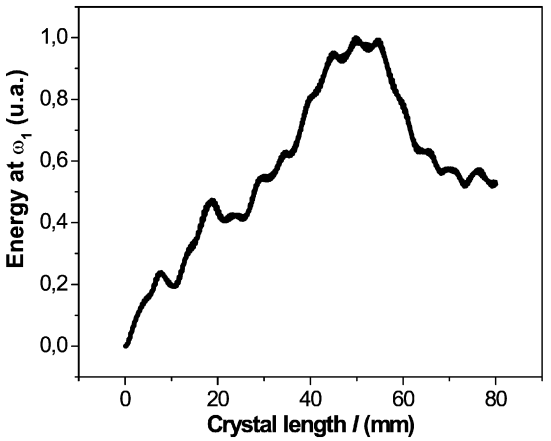

Fig. 9. Evolution of the amount of DFG power extracted from a GaAs plate as a function of the plate length for a (1.9 μm, 2.3 μm) $\underset{\text{DFG}}{\longrightarrow}$ 11 μm process: result of the guided wave calculation. The general features of Fig. 5 are obtained.

p_0 is a normalizing power constant which is such that the amplitude of the Poynting vector $\vec{S}$ given by:

$$S = \frac{1}{\mu_0} \int_{-\infty}^{+\infty} \vec{E} \times \vec{B}\, \mathrm{d}x = \frac{\beta_l^{\omega}}{2\omega\mu_0} \int_{-\infty}^{+\infty} \left| E_{l,y}^{\omega} \right|^2 \mathrm{d}x = p_0 \tag{15}$$

which corresponds to a power of 1 W m^{-1} in the y direction. $S_{l,l',m}$ is the overlap integral between the modes:

$$S_{l,l',m} = \int_{-\infty}^{+\infty} E_{l,y}^{\omega}(x) E_{l',y}^{\omega}(x) E_{m,y}^{2\omega}(x)\, \mathrm{d}x \tag{16}$$

and $\delta\beta_{l,l',m}$ are the mismatch in the propagation constants:

$$\delta\beta_{l,l',m} = \beta_m^{2\omega} - \beta_l^{\omega} - \beta_{l'}^{\omega} \tag{17}$$

The normalization constant in Eq. (14) is such that the total amount of harmonic power generated by unit length along y axis is given by the summation over each mode contribution m:

$$P_{2\omega}(z) = \sum_m \left| A_{m,y}^{2\omega}(z) \right|^2 \tag{18}$$

A careful examination of Eq. (14) shows that the different phase matching conditions derived in Section 2 can be found again in the guided wave approach. For instance, the nonlinear Law of reflection (10), the phase matching condition (5) and (6) may be derived after some cumbersome series expansion and algebra.

Fig. 8(b) shows the calculated evolution of the SHG signal in the GaAs plate for a (8 μm) $\underset{\text{SHG}}{\longrightarrow}$ 4 μm interaction. One clearly sees that, due to the different effects described in Section 3.3, the SHG gradually walk off from the fundamental waves and fills the whole volume of the plate. Fig. 9 shows the output energy as a function of plate length for a (1.9 μm, 2.3 μm) $\underset{\text{DFG}}{\longrightarrow}$ 11 μm interaction. The general features of experimental results (as seen in Fig. 5) are observed, i.e., a destructive recombination of the waves after some distance due to the different walk off processes.

4. Conclusions

Fresnel phase matching is a very versatile and universal way to phase match second order parametric interaction, particularly in isotropic materials where birefringence phase matching is not feasible. Limitations come mostly from walk-off effects, due to Goos–Hänchen shifts and nonlinear reflection at the interfaces. A guided wave description has been developed, which does take into account all these phenomena in a built in way and thus will allow optimum structures to be designed and tested in a near future.

References

[1] E. Rosencher, A. Fiore, B. Vinter, V. Berger, P. Bois, J. Nagle, Science 271 (1996) 168.
[2] R.L. Sutherland, Handbook of Nonlinear Optics, Marcel Dekker, Inc., New York, 1996.
[3] E. Rosencher, B. Vinter, Optoelectronics, Cambridge University Press, Cambridge, 2002.
[4] J.A. Armstrong, N. Bloembergen, J. Ducuing, P.S. Pershan, Phys. Rev. 127 (1962) 1918.
[5] H. Komine, W.H. Long, J.W. Tully, E.A. Stappaerts, Opt. Lett. 23 (1998) 661.
[6] R. Haidar, N. Forget, P. Kupececk, E. Rosencher, J. Opt. Soc. Am. B 21 (2004) 1522.
[7] M. Born, E. Wolf, Principles of Optics, 1964.
[8] F. Goos, M. Hänchen, Ann. Phys. 1 (1947) 333.
[9] N. Bloembergen, P.S. Pershan, Phys. Rev. 128 (1962) 606.
[10] Marcuse, Theory of Dielectric Optical Waveguides, Academic Press, London, 1974.
[11] A. Yariv, IEEE J. Quant. Electron. QE-9 (1973) 919.